

## Dynamical studies of gratings formed in polymer-dispersed liquid crystal films doped with a guest-host dye

Andy Y.-G. Fuh,\* M.-S. Tsai, C.-R. Lee, and Y.-H. Fan

*Department of Physics, National Cheng Kung University, Tainan, Taiwan 701, Republic of China*

(Received 6 December 1999)

This study investigated the dynamic behavior of the first-order diffraction efficiency of gratings formed in polymer-dispersed liquid crystal (PDLC) films doped with a guest-host dye. PDLC films were fabricated using various LC-polymer mixing ratios, and written with various powers. Experimental results indicated that several peaks appeared in the curve of the first-order diffraction efficiency versus time. According to the light scattering study, we believe that the first peak was due to the superposition of density and absorption gratings. The density grating was associated with the spatially varied molecular weight of polymer molecules across the sample, and the absorption grating resulted from the spatially varied density of free electrons. The other peaks were caused by the superposition of the absorption and phase gratings. The phase grating was generated by the formation of a periodic structure of polymer-rich and LC-rich regions in the sample. This study also proposes a model to explain these experimental results. Moreover, the theory derived from this model correlates well with the experimental results, allowing us to determine the amplitude of the final grating.

PACS number(s): 42.70.Df, 42.70.Ln, 42.70.Jk

### I. INTRODUCTION

New holographic recording materials based on photopolymerizable systems have significantly contributed to the recent growth of holographic applications, particularly in data storage [1], optical interconnections [2], and the use of holographic interferometry [3] for studying local deformations and microdisplacements. A holographic grating can be made in photopolymer films via a single-step process at a relatively fast speed. In addition, the selection of different sensitizing dyes allows several different optical recording wavelengths to be utilized. The feasibility of developing and applying electrically [4–7] and optically [8] switchable holographic gratings has gained increasing interest [4,5]. Of particular interest has been the use of films of polymer-dispersed liquid crystal (PDLC) materials.

A PDLC consists of micro-sized liquid crystal droplets dispersed in a polymer matrix [9]. PDLC films scatter light and appear opaque in the off state, while they are transparent in the on state. This change in opacity can be achieved by applying an ac electrical field (typically  $\sim 10^4$  V/cm) across the film. In this study, we examine the dynamic behavior of PDLC gratings. Moreover, we propose a mechanism describing the dynamic formation of the grating based on the results obtained from light scattering experiments. The diffraction theory derived from this model correlates qualitatively with the experimental results.

### II. EXPERIMENT

The liquid crystal, monomer, cross-linking agent, and photoinitiator employed in this experiment were E7 (Merck), dipentaerythritol pentaacrylate (DPPA; Polysciences), 1-vinyl-2-pyrrolidinone (NVP; Aldrich), and *N*-phen-

ylglycine (NPG; Aldrich), respectively. A small amount of a photoinitiator dye rose Bengal (RB) and of a guest-host dye G-206 (Nippon Kankoh-Shikiso Kenkyusho) was added to the PDLC mixtures in the sample. RB dye absorbs green-blue light, resulting in an excited singlet state followed by fluorescence or intersystem crossing to the triplet state. The RB triplet undergoes an electron-transfer reaction in which NPG functions as an electron donor, producing an NPG free radical and then initiates the polymerization of DPPA and NVP [10]. A separate experiment indicated that the polymerization reaction in a PDLC film proceeds slowly when a small amount of G-206 dye is added (result not shown). According to our previous study [8], adding a small amount of G-206 dye could absorb an Ar<sup>+</sup> laser pulse and induce thermal expansion, subsequently creating a better orientation of LC molecules in the PDLC grating. Thus, the refractive difference between the LC-rich and polymer-rich stripe increases. This is commonly referred to as an optically switchable grating.

Here, a mixture of 8 wt % of NVP, 0.5 wt % of NPG, 0.7 wt % of RB, and 0.7 wt % of G-206 was prepared and used to make three PDLC compounds by adding various E7 and DPPA concentrations. They were (1) 20 wt % of E7, 70.1 wt % of DPPA, (2) 30 wt % of E7, 60.1 wt % of DPPA, and (3) 40 wt % of E7, 50.1 wt % of DPPA. Drops of the homogeneously mixed compound were then sandwiched between two indium tin oxide (ITO) coated glass slides separated by 36- $\mu$ m-thick plastic spacers to form a sample.

The experimental setup and its principles to form PDLC gratings are based on previous studies [5]. Briefly, two TE polarized writing beams  $\mathbf{E}_1$  and  $\mathbf{E}_2$  derived from an Ar<sup>+</sup> laser ( $\lambda = 514.5$  nm), intersected at an angle  $\theta \sim 3^\circ$ . They were unfocused, each having a beam diameter  $\sim 4$  mm. They had an approximately equal power, which was varied in this experiment. During writing, an unpolarized He-Ne laser was introduced in the plane determined by beams  $\mathbf{E}_1$  and  $\mathbf{E}_2$  to probe the writing region of the sample. The intensity of one

\*Author to whom correspondence should be addressed. Email address: andyfuh@mail.ncku.edu.tw

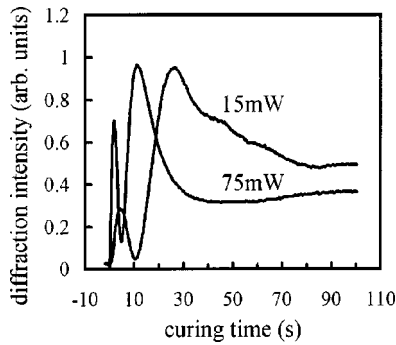


FIG. 1. Dynamic changes of the first-order diffraction efficiency for a PDLC sample with an E7 concentration  $\sim 20$  wt % as a function of time with writing powers of 15 and 75 mW.

of the first-order diffracted beams was monitored as the grating was being formed

The development of a PDLC system during the curing process provides further insight into the dynamic behavior of the grating formation. We used a light scattering method [5] to determine the beginning of phase separation in this PDLC system. Both an  $\text{Ar}^+$  laser and a He-Ne laser were simultaneously beamed onto the sample. These two beams made an angle  $\sim 1.5^\circ$  and overlapped at the sample. The He-Ne laser was used to probe the dynamical change of the sample's transparency when it was cured by the  $\text{Ar}^+$  laser. The onset of turbidity can be considered the beginning of phase separation in this PDLC system.

The morphologies of written gratings were examined using atomic force microscopy (AFM). LC molecules were removed from these samples by placing the cells in a hexane solvent [7].

### III. RESULTS AND DISCUSSION

Figure 1 shows the measured curves of the first-order diffraction intensities for a PDLC grating with a LC concentration of  $\sim 20$  wt % as a function of time with writing powers of 15 and 75 mW. Notably, these two curves are similar since each has two peaks. When the writing power is higher, the times at which the two peaks appear are earlier. Meanwhile, the corresponding peak diffraction intensities are larger.

The curves shown in Fig. 2 are similar to those depicted in Fig. 1. These curves represent the results obtained from gratings with E7 concentrations of  $\sim 30$  and  $\sim 40$  wt %, and samples written with power  $\sim 50$  mW. The inset in Fig. 2 is the magnification for the curing time in the initial 4 s. The apparent dynamical diffraction behavior is different for PDLC films with varying E7 concentration, as a small peak appears at  $\sim 1.8$  s for the film with E7  $\sim 30$  wt %, while it disappears for the film containing 40 wt % E7.

Figure 3 shows the results of a light scattering experiment for the samples with E7 concentrations of 20, 30, and 40 wt % as a function of time, and cured with a power  $\sim 25$  mW. There is an appearance of turbidity in these three samples. More LC droplets or domains are formed as the LC concentration increases, causing a greater drop in transmission for a sample with a higher LC concentration. A minimum is observed at early time of the curves in Fig. 3. In

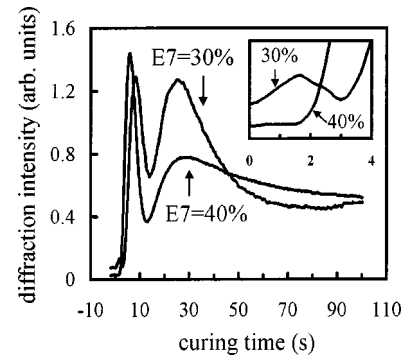


FIG. 2. Dynamic changes of the first-order diffraction efficiency for PDLC samples with E7 concentrations 30 and 40 wt % as a function of time. The samples were written with writing beams of power  $\sim 50$  mW. The inset is the magnification for the curing time in the initial 4 s.

addition, the depth of the minimum depends on the LC concentration and its curing power. We believe that this minimum is due to the absorption of light by the photoinduced free electrons during the initiation of polymerization. In our photopolymer system, light absorbed by the photoinitiator RB results in an excited singlet state followed by fluorescence or intersystem crossing to a triplet state. The RB triplet undergoes an electron-transfer reaction in which NPG functions as an electron donor, producing an NPG radical that initiates prepolymer polymerization. The transmission of light is restored to its initial value since the free electrons disappear when the coinitiator NPG has been completely consumed. The formation of LC droplets or domains starts earlier in a sample with higher LC concentration. The scattering of light by these LC droplets or domains then makes the minimum less visible, as shown in Fig. 3.

A dynamic light scattering experiment was performed to verify the above hypothesis. A cw  $\text{Ar}^+$  laser with a power  $\sim 300$  mW was chopped and incident normally onto a sample. The laser beam was then used as a pump beam to initiate polymerization of the prepolymers in the mixtures. An unpolarized He-Ne laser (5 mW) was introduced simultaneously to probe the excited region of the sample when applying the pump-beam pulses. The angle between these two beams was  $\sim 1.5^\circ$ . A current sensitive amplifier (EG&G 181) was connected to the ITO electrodes of the sample to monitor the induced current. Figure 4(a) summarizes the

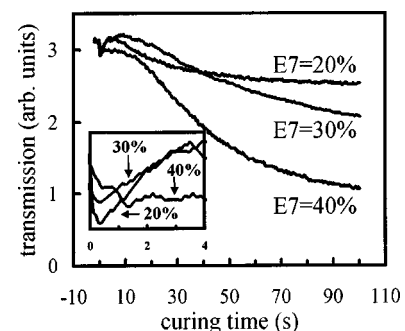


FIG. 3. Results obtained from light scattering experiment for PDLC samples with E7 concentrations of 20, 30, and 40 wt % as a function of time, and cured with a power  $\sim 25$  mW. The inset is the magnification for the curing time in the initial 4 s.

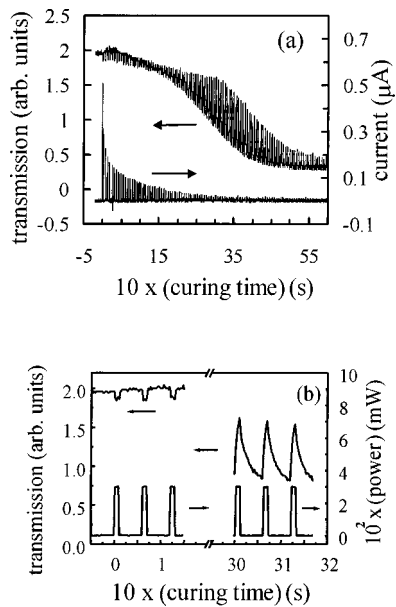


FIG. 4. (a) Dynamic change of the probe-beam transmission (upper curve) and the induced current (bottom curve) for a PDLC film having a LC concentration  $\sim 40$  wt % in response to a pump beam chopped with an off- to on-time ratio of 5:1. The period is 6 s. (b) Replot of the partial upper curve of, both before and after the turning point, with a relatively large horizontal scale. The chopped pump pulses are shown in the bottom curve.

measured results of the probe-beam transmission and the induced current for a pump beam chopped with a period of 6 s and an on- to off-time ratio of 1:5 for a sample having a LC concentration of 40 wt %. Interestingly, a turning point appears in the curve representing the probe beam's transmission versus curing time. A partial upper curve from Fig. 4(a) replotted and depicted in Fig. 4(b) illustrates the transmission of the probe beam both before and after the turning point in greater detail, including the pump pulses. The transmission of the probe beam is lower when the pump beam (on time) illuminates the sample than when the sample is not illuminated (off time) before the turning point. However, the reverse is true after the turning point. Notably, a significant current was induced for this sample, indicating that this was a dc current with the negative charges moving against the propagation direction of the pump/probe beam.

Previous investigations have assumed that the lower transmission experienced by the probe beam during the illumination of the sample by the pump beam before the turning point is due to the absorption of light by the mobile charges. We believe that the mobile charges are free electrons. Their existence is supported by the measurement of the induced current. The induced dc current would separate positive and negative charges. They may be trapped by the polymer and form a polarization field. When the field is strong enough, it aligns the LC molecules with their long axes along the pump-beam direction. Some of the trapped charges may recombine when the pump beams are off. This results in a lower electric field, and causes the relaxation of the alignment effect. Consequently, the probe-beam transmission should be higher when the pump beam illuminates the sample (on time) than during the off time. Next, the "homeotropically" aligned sample was optically verified using a

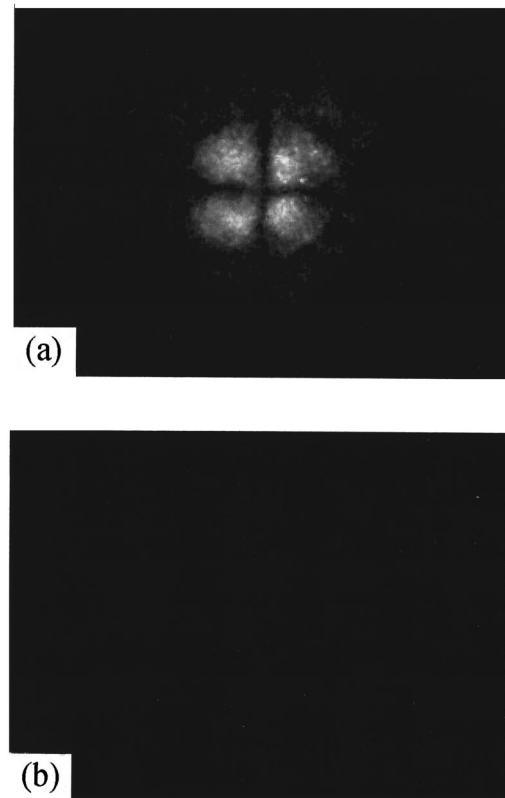


FIG. 5. Patterns during (a) the on time and (b) the off time of the probe beam at approximately the time of the maximum modulation in Fig. 4(a). Notably, the film did not retain the homeotropic order after the pump pulse was off.

typical arrangement for conoscopic inspection. Figure 5(a) shows the observed patterns corresponding approximately to the maximum modulation in Fig. 4(a). Notably, the film did not retain the homeotropic order of LC molecules after the pump pulse was off [Fig. 5(b)].

The above two effects on the transmission of the probe beam, i.e., the charge effect and the LC alignment effect, competed with each other during polymerization of the LC-prepolymer mixtures. The former occurred in the initiation stage, while the transmission of the probe beam was observed to be lower when the sample was being illuminated with the pump pulse before the turning point, as shown in Fig. 4(b). The LC alignment effect became more pronounced as the polymerization continued. The difference in the probe-beam transmission when the sample was illuminated with and without the pump beam was zero when the two effects were equal in amplitude at the time of the turning point, as shown in Fig. 4(a). The LC alignment effect became dominant after the turning point. Therefore, the probe-beam transmission was higher when the sample was being illuminated with the pump beam, as shown in Fig. 4(b).

A model for the dynamical formation of PDLC gratings is proposed based on the results obtained from the light scattering experiment. A diffraction equation is derived to fit the results shown in Figs. 1 and 2. The two writing beams  $\mathbf{E}_1$  and  $\mathbf{E}_2$  set up a sinusoidal interference light pattern. Since photopolymerization is preferentially initiated in the high-intensity regions, a spatial pattern of monomer concentration occurs across the film. Consequently, there is a diffusion of

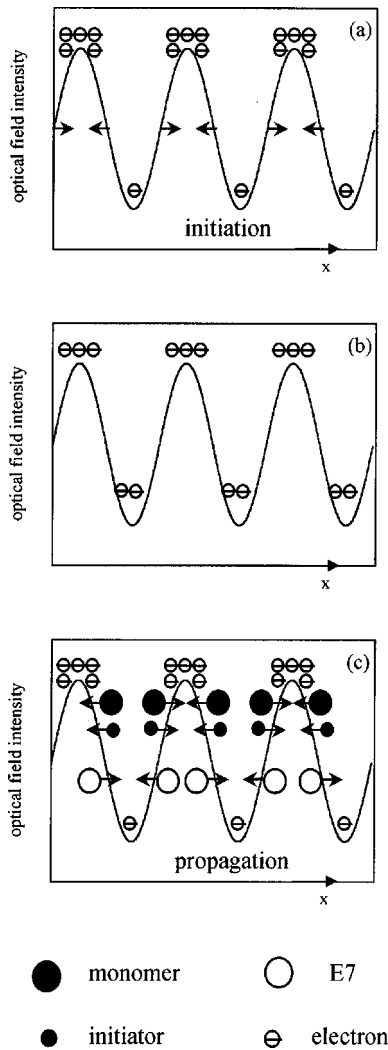


FIG. 6. The proposed model for the dynamic formation of PDLC gratings. The three stages during polymerization are (a) initiation, (b) end of initiation, and (c) propagation.

monomer molecules toward the high-intensity regions [11]. The molecular weight of the polymers in the high-intensity regions increases (because of cross linking) to a much greater extent than that of polymers in the low-intensity regions. Therefore, the intensity interference pattern produces a refractive index grating that can be associated with the spatially varying molecular weight of the polymer molecules, termed the density grating. The spatially varying photopolymerization rate simultaneously resulted in an absorption grating that can be associated with the spatially varying density of the photoinduced free electrons, as shown in Fig. 6(a). The amplitude of the absorption grating decreases due to the depletion of the initiator in the high-intensity regions as the polymerization continues. Also, some of the free electrons diffuse to the low-intensity regions as pictured in Fig. 6(b). Photopolymerization also results in the diffusion of initiators toward the high-intensity regions. As a result, polymerization continues further in the high-intensity regions, and gives the secondary absorption grating. On the other hand, liquid crystal molecules are not consumed, and their chemical potential increases in the high-intensity regions over that in the low-intensity regions due to the consumption of monomers. Hence there is a diffusion of LC, molecules

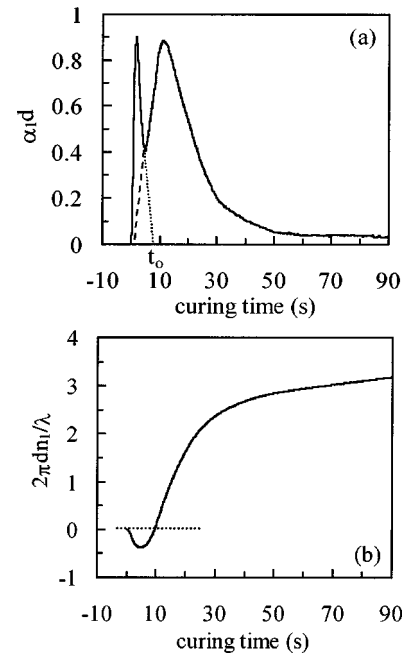


FIG. 7. Variation of the function  $\alpha_1(t)$ , which is the difference in the light absorption coefficient between the high- and low-intensity regions, with respect to the curing time for a PDLC sample with an E7 concentration  $\sim 20$  wt %. The writing power was  $\sim 75$  mW. (b) The curve of  $n_1(t)$ , which is the refractive difference between the low- and high-intensity regions, obtained from Eq. (3).

from the high-intensity regions toward the low-intensity ones to equalize the chemical potential everywhere in the writing area, as depicted in Fig. 6(c). This diffusion is then followed by the formation of a phase grating that is associated with the periodic arrangement of polymer-rich material in the high-intensity regions and LC-rich material in the low-intensity regions. The refractive index in the LC-rich regions is greater than that in the polymer-rich regions. Thus, the phase grating is phase shifted by  $180^\circ$  with respect to the density grating.

Let  $\alpha_1(t)$  represent the difference in the absorption coefficient of light between the high- and low-intensity regions. Based on the above analysis, we speculate that the function  $\alpha_1(t)$  has the shape depicted in Fig. 7(a) for the sample with an E7 concentration  $\sim 20$  wt % and written with a power  $\sim 75$  mW. The product of the first peaked value of  $\alpha_1(t)$  shown in Fig. 7(a) and the cell thickness,  $\alpha_1^{\max}d$ , is assumed to be  $\sim 0.85$ , i.e.,  $\alpha_1^{\max} \sim 235 \text{ cm}^{-1}$ . Notably, the shape of  $\alpha_1(t)$  used in the simulations of other samples is similar to that shown in Fig. 7(a). But some adjustments are made to account for the variations in LC concentration in the sample and in its writing power. The amplitude of the absorption grating for a sample written with a higher power is expected to increase as supported by the results shown in Fig. 1. Thus, the value of  $\alpha_1^{\max}d$  is increased accordingly. The diffusion of both the LC molecules and the monomers is easier due to a lower viscosity as the LC concentration increases. Thus, the absorption grating will be rapidly quenched as seen from the comparison of Figs. 1 (E7, 20 wt %) and 2 (E7, 30 and 40 wt %). The peak appearing at early time in Fig. 1 is not evident in Fig. 2. Thus,  $\alpha_1^{\max}d$  is smaller in a sample having a higher E7 concentration. The values of  $\alpha_1^{\max}$  used in the PDLC grating simulations have various LC concentrations

TABLE I. Values of  $\alpha_1^{\max}$  and  $n_1^{\max}$  used in the simulations of the dynamic behavior of the PDLC gratings with various LC concentrations, and written with various powers.  $\alpha_1^{\max}$  is the first-peak value of  $\alpha_1(t)$  shown in Fig. 7(a), and  $n_1^{\max}$  is the amplitude of the final grating.

LC concentration (wt %)	Laser power (mW)	$\alpha_1^{\max}$ ( $\text{cm}^{-1}$ )	$n_1^{\max}$
20	15	140	0.008
20	75	235	0.008
30	50	50	0.015
40	50	10	0.019

and are written with various powers as listed in Table I.

The PDLC gratings formed were of the Raman-Nath type since the angle between the two writing beams in the present experiment was  $\sim 3^\circ$  [12]. The probe beam was normally incident onto the sample, so the amplitude of the first-order diffraction wave,  $A_1(t)$ , can be written as [13,14]

$$A_1(t) = \frac{1}{2\pi} \int_0^{2\pi} T(t) e^{-d\alpha_1(t)g(\xi)} e^{-i(2\pi d/\lambda)n_1(t)f(\xi)} e^{-i\xi} d\xi, \quad (1)$$

where  $\alpha_1(t)$  is the difference in light absorption coefficient between the high- and low-intensity regions,  $n_1(t)$  is the refractive difference between the low- and high-intensity regions,  $T(t)$  is the transmission of the sample,  $g(\xi)$  is the shape of the absorption grating,  $f(\xi)$  is the shape of the refractive grating, and  $\lambda$  (632.8 nm) is the wavelength of the probe beam (He-Ne laser) in vacuum. The square of the absolute value of  $A_1(t)$  gives the first-order diffraction intensity  $I_1(t)$ , i.e.,

$$I_1(t) = |A_1(t)|^2. \quad (2)$$

Notably,  $\alpha_1(t)$ ,  $n_1(t)$ , and  $T(t)$  must be found to obtain  $A_1(t)$  in Eq. (1). As mentioned above, the function  $\alpha_1(t)$  is assumed to have the shape shown in Fig. 7(a). Then,  $n_1(t)$  can be obtained as follows. First we extend the curves on the two sides of the minimum point between the two peaks shown in Fig. 7(a) to the horizontal axis.  $\alpha_1(t)$  consists of two peaks. Based on the model described above, the first peak  $\alpha_1^{(1)}(t)$  gives the density grating  $n_d(t)$ , and the second peak  $\alpha_1^{(2)}(t)$  gives the phase grating  $n_p(t)$ . Moreover, they are  $180^\circ$  out of phase. Let  $M(t)$  be the polymerization rate; then it is reasonable to write  $n_1(t)$  as

$$n_1(t) = n_p(t) - n_d(t) \propto \int_0^t M(t) dt \propto \int_0^t [\alpha_1^{(2)}(t) - \alpha_1^{(1)}(t)] dt. \quad (3)$$

If the proportional constant in Eq. (3) is unity, the  $n_1(t)$  obtained with a LC concentration of 20 wt% is shown in Fig. 7(b). The final value of  $n_1(t)$ ,  $n_1^{\max}$ , is assumed to be  $\sim 0.008$ . Note that, since  $n_1(t)$  is initially negative, becoming positive later, the refractive index is initially higher in the high-intensity regions (density grating). The phase grating later dominates, and  $n_1(t)$  becomes positive.  $n_1^{\max}$  is 0.015 and 0.019 for PDLC gratings with E7 concentrations of 30

and 40 wt% as listed in Table I. This assumption is reasonable, since the higher the LC concentration, the richer the LC-rich regions are in each sample. Booth estimated  $n_1$  in photopolymer material as  $\sim 5 \times 10^{-3} - 10^{-2}$  [15]. Our estimated value of  $n_1^{\max}$  in PDLC gratings is 2–4 times larger than that in photopolymers but is reasonable for the following reasons

(1) The material used in Ref. [15] is a pure photopolymer as compared to a LC-polymer mixture in the present case. The ordinary and extraordinary refractive indices  $n_o$  and  $n_e$  of E7 are 1.522 and 1.746, respectively. Consequently, the LC-rich regions in PDLC gratings have an average index of  $(n_o + n_e)/2 \sim 1.63$ , if LC's are completely phase separated from polymers, which is larger than the index of the polymer-rich regions,  $n_p \sim 1.52$ .

(2) The grating spacing in the present case is  $\sim 10 \mu\text{m}$ , which is larger than that reported in Ref. [15]. The larger grating spacing implies a higher grating amplitude.

(3) A small amount of guest-host dye G-206 is added in the present samples since our previous study demonstrated that adding a small amount of G-206 dye could enhance the refractive difference between the LC-rich and polymer-rich stripes [8].

As mentioned above, the higher is the LC concentration in the sample, the more the LC droplets form in LC-rich regions in a PDLC grating (or in a typical PDLC film). We would expect that both the  $n_1^{\max}$  (PDLC grating) and light scattering (PDLC film) would be proportional to the LC concentration in the sample. The transmission of the samples  $T(t)$ , as shown in Fig. 3, can be then approximately fitted by

$$T(t) = 1 - K \frac{|n_1(t)|}{n_1^{\max}}, \quad (4)$$

where  $K$  is a constant, which is proportional to the LC concentration in the sample.  $K$  is estimated through fitting of Fig. 3 to be  $\sim 0.1, 0.3, \text{ and } 0.5$  for PDLC films with E7 concentrations of 20, 30, and 40 wt%, respectively.

The grating morphologies of PDLC gratings were studied using atomic force microscopy. We split the cell and put it in hexane solvent to remove the liquid crystals. Special care was taken not to disturb the grating morphology during splitting. Using AFM, we then studied the polymer structure of the grating. This technique allows us to directly measure the shape of the grating qualitatively. The results (not shown) reveal that the grating shape is approximately sinusoidal for the sample with an E7 concentration of 20 wt%. The shape becomes squarelike when the E7 concentration is increased to 40 wt%. As a result, the functions  $f(\xi)$  and  $g(\xi)$  are assumed to be  $\sin \xi$ ,  $\sin \xi + \frac{1}{3} \sin 3\xi$ , and  $\sin \xi + \frac{1}{3} \sin 3\xi + \frac{1}{5} \sin 5\xi$  for the PDLC gratings with E7 concentrations of 20, 30, and 40 wt%, respectively.

Following the above discussion,  $\alpha_1(t)$  [from Fig. 6(a)],  $n_1(t)$  [Eq. (3)], and  $T(t)$  [Eq. (4)] enable  $A_1(t)$  to be calculated from Eq. (1). The simulation results of the first-order diffraction efficiency as a function of time for the sample with an E7 concentration of  $\sim 20$  wt% with writing powers of 15 and 75 mW are shown in Fig. 8. Figure 9 shows the simulated results for the samples with E7 concentrations of 30 and 40 wt%, and written with a power 50 mW. A com-

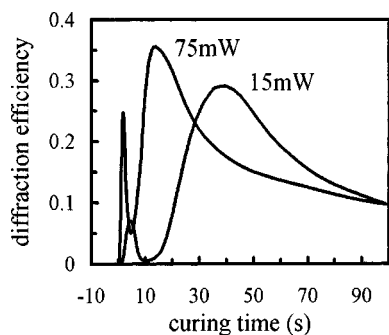


FIG. 8. The simulated results of the first-order diffraction efficiency versus time for the samples that give the experimental results shown in Fig. 1.

parison of Figs. 8 and 9 with Figs. 1 and 2 confirms that the simulated results agree with the experimental results.

The dynamical behaviors of holographic gratings formed in PDLC films doped with a guest-host dye were examined in this paper. The light scattering and dynamical polymerization effects of the samples were also studied. A model was proposed to explain the results based on the results obtained from the latter experiments. The theory derived from this model qualitatively correlates with the experimental results. The density grating associated with the spatially varying molecular weight of the polymer across the sample plays an important role in the early time of the grating formation. However, the phase grating resulting from the formation of a periodic structure of LC-rich and polymer-rich regions due to the phase separation dominates later. Moreover, the amplitude of the final phase grating,  $n_1^{\max}$ , can be obtained through fitting.

Figures 1 and 2 are the results obtained using an unpolarized probe beam. The consequences of changing the polarization of the probe beam were also examined. In these experiments, a PDLC grating with 40 wt % E7 was used. The experimental conditions were made identical to those that gave the result shown in Fig. 2 (E7=40 wt %) except for the

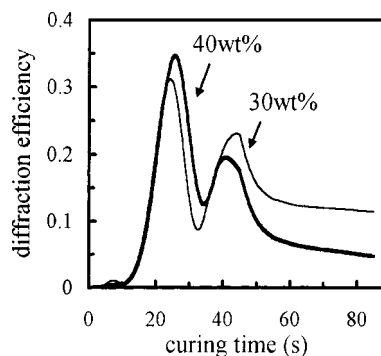


FIG. 9. The simulated results of the first-order diffraction efficiency versus time for the samples that give the experimental results shown in Fig. 2.

polarization of the probe beam. An unpolarized He-Ne laser was normally incident onto the sample through a polarizer, which can be rotated to change the polarization of the probe beam. Let  $\varphi$  be the angle made between the polarizations of the probe beam and the writing beams. The shape of the measured curves for different angles  $\varphi$  is similar to that shown in Fig. 2 with 40 wt % E7, but the amplitude of the final grating decreases as  $\varphi$  increases. The change of the grating's amplitude is  $\sim 7\%$  when the angle  $\varphi$  changes from  $0^\circ$  to  $90^\circ$ . This indicates that the orientation of LC molecules in the LC-rich regions is parallel to the grating's stripe direction (which is also the polarization direction of the writing beams). However, the orientational order is low, since the decrease of the grating's amplitude for the probe beam polarized with an angle from  $\varphi=0^\circ-90^\circ$  is small.

#### ACKNOWLEDGMENTS

The authors would like to thank the National Science Council (NSC) of the Republic of China for financially supporting this research under Contract No. NSC 88-2112-M-006-012. M.-S.Tsai would like to thank Z.-Y. Su for his assistance in the computer simulation.

- 
- [1] P. Hariharan, *Optical Holography* (Cambridge University Press, London, 1984).
  - [2] P. C. Mehta and V. V. Rampal, *Lasers and Holography* (World Scientific, Singapore, 1993).
  - [3] C. M. Vest, *Holographic Interferometry* (Wiley, New York, 1979).
  - [4] R. L. Sutherland, V. P. Tondiglia, and L. V. Natarajan, *Appl. Phys. Lett.* **64**, 1074 (1994).
  - [5] A. Y.-G. Fuh, T.-C. Ko, M.-S. Tsai, C.-Y. Huang, and L.-C. Chien, *J. Appl. Phys.* **83**, 679 (1988).
  - [6] V. P. Tondiglia, L. V. Natarajan, R. L. Sutherland, T. J. Bunning, and W. W. Adams, *Opt. Lett.* **20**, 1325 (1995).
  - [7] A. Y.-G. Fuh, M.-S. Tsai, C.-Y. Huang, T.-C. Ko, and L.-C. Chien, *Opt. Quantum Electron.* **28**, 1535 (1996).
  - [8] A. Y.-G. Fuh, M.-S. Tsai, L.-J. Huang, and T.-C. Liu, *Appl. Phys. Lett.* **74**, 2572 (1999).
  - [9] B. Bahadur, *Liquid Crystals: Applications and Uses* (World Scientific, Singapore, 1990), Vol. 1.
  - [10] R. L. Sutherland, L. V. Natarajan, V. P. Tondiglia, and T. J. Bunning, *Chem. Mater.* **5**, 1533 (1993).
  - [11] T. J. Bunning, L. V. Natarajan, V. Tondiglia, R. L. Sutherland, D. L. Vezie, and W. W. Adams, *Polymer* **36**, 2699 (1995).
  - [12] R. W. Boyd, *Nonlinear Optics* (Academic, London, 1992).
  - [13] R. Magnusson and T. K. Gaylord, *J. Opt. Soc. Am.* **68**, 806 (1978).
  - [14] R. Magnusson and T. K. Gaylord, *J. Opt. Soc. Am.* **68**, 809 (1978).
  - [15] B. L. Booth, *Appl. Opt.* **14**, 593 (1974).